Resonant electron scattering by molecules adsorbed on rare-gas films: N_2 vibrational excitation via the N_2^- ($^2\Pi_g$) resonance

D. C. Marinica, D. Teillet-Billy, and J. P. Gauyacq
Laboratoire des Collisions Atomiques et Moléculaires, Unité Mixte de Recherche CNRS-Université Paris Sud UMR 8625, Bât 351, Université Paris-Sud, 91405 Orsay Cedex, France

M. Michaud and L. Sanche
Groupe des Instituts de Recherche en Santé du Canada en Sciences des Radiations, Université de Sherbrooke, Sherbrooke, Québec, Canada J1H 5N4

(Received 28 November 2000; published 3 August 2001)

Vibrational excitation by low-energy electron impact of N_2 molecules physisorbed on rare-gas films is studied both experimentally and theoretically in the energy range of the N_2^- ($^2\Pi_g$) resonance. The experimental measurements provide the energy dependence of the vibrational excitation (i.e., the excitation function) and the overtone ratio for solid films of Ar with thickness varying between 1 and 32 monolayers condensed on a Pt substrate. The oscillations in the excitation function (i.e., the ''boomerang'' structure) are deeply modified by the presence of the rare-gas film. The theoretical study, using a dielectric continuous medium modeling of Ar and Xe rare-gas films, shows that the experimental observations are linked to a lowering of the energy and an increase in the lifetime of the resonance on the solid rare-gas film, which strongly influences the boomerang oscillations. The various features observed in the excitation function are attributed to the presence of a potential barrier at the dielectric-vacuum interface.

DOI: 10.1103/PhysRevB.64.085408 PACS number(s): 79.20.−m, 79.60.Dp, 34.80.Gs

I. INTRODUCTION

A major challenge in surface science is to induce and control chemical reactions at interfaces both at the macroscopic and microscopic levels. Along the reactive route from reactants to products, transient species can be formed. Controlling the formation and decay of these transient intermediate states would allow one to act more efficiently on the entire reactive process. A large class of surface reactions involves a charge transfer as an intermediate step. Transient negative ions (i.e., electron resonances) play an important role in reactions and in particular in surface reactions.[1–4] This has been clearly demonstrated for excitation, fragmentation, and desorption processes. In all of these processes, the formation of a transient negative ion allows the transfer of energy from electronic motion to nuclear motion. Given a resonance vibrational coupling, the efficiency of this transfer depends on the resonance lifetime, which can be strongly dependent on the molecular environment. Numerous studies have focused on resonance-mediated electron impact vibrational excitation and dissociative attachment of molecules physisorbed on bare metal surfaces; the effect of the neighboring metal on the resonance characteristics (energy position and width) as well as on the energy transfer itself have been discussed. In the present work, we investigate both experimentally and theoretically the dynamics of vibrational excitation by low-energy electron impact of N_2 molecules physisorbed on an insulating rare-gas film.

Vibrational excitation of N_2 molecules by low-energy electron impact is dominated by the N_2^- ($^2\Pi_g$) resonance. In the free molecule, this resonance is located at 2.3 eV and its width is around 0.4 eV at the N_2 equilibrium position, which corresponds to a lifetime of the order of the vibrational period. This resonance is not sufficiently long lived to allow the quantization of its nuclear motion. The resonance decays by electron emission in the course of nuclear motion, and the molecule only vibrates once during the collision. The interference between electron emission at different times of the vibrational motion leads to the appearance of so-called ''boomerang'' oscillations in the energy dependence of the vibrational excitation cross sections. Herzenberg theoretically described these in the 1970s.[5,6] The boomerang pattern is different for each final vibrational channel. It is extremely sensitive to the characteristics of resonant scattering, which makes the N_2 molecule a very appealing probe to study perturbations introduced by the environment on a transient negative ion.

Quite a few theoretical and experimental studies have been devoted to the case of transient negative ions on bare metal surfaces. For free-electron metals, the dominant perturbation is caused by the image charge interaction that results in the lowering of the energy position of the resonance and in the increase of the resonance width. This was recognized very early[7–10] and led to qualitative discussions of various experimental results on the resonant vibrational excitation of physisorbed molecules.[11–15] As for theoretical studies of the electron impact vibrational excitation process itself,[16] they revealed that besides the changes in the resonance energy and width, the presence of a metal surface introduces an asymmetry in space that strongly influences the excitation process and in particular the overtone excitation. In the case of non-free-electron metal surfaces, the peculiarities of the band structure of a metal have also been shown to influence the position and width of transient states interacting with the metal. Rous[17] showed that it could lead to an increase or a decrease of the resonance width.

Transient states in an insulating environment also re-

ceived some attention. Condensed gases and in particular rare gases provide a simple system, the prototype of insulating thin films, modifying the electronic environment of a molecule. Dissociative electron attachment (DEA) in condensed gases has been studied in detail experimentally either in the case of a pure condensed molecular gas or with a rare gas used to dilute the active molecule or separate it from the substrate.[18] Energy shifts of the DEA reaction and the change of selection rules, as well as reactions in the condensed layers induced by DEA have been reported.[19] Theoretical studies are scarcer. The DEA process in halogen containing molecules adsorbed on rare-gas solid (RGS) films has been modeled by simply introducing an energy shift of the transient negative ion into the DEA treatment of the free molecule.[20,21] This accounted well for the experimentally observed increase of the DEA cross section by several orders of magnitude when going from the free molecule to the adsorbed system.[20,21]

Transient electronic states analogous to those involved in resonant electron scattering are present in other experiments. Recently, the development of time-resolved two-photon photoemission (TR-2PPE) experiments in the femtosecond range allowed a direct study of some of these states. These are located below the vacuum level in contrast to the molecular resonances probed by electron scattering. In the case of adsorbate-induced states on surfaces such as Cu(111), very-long-lived states have been observed;[22,23] this feature has been shown to be related to the effect of the electronic band structure and more specifically to the presence of a projected band gap that blocks the electron transfer between the adsorbate and the substrate.[24] Image states at surfaces and in particular their perturbation by an insulating layer on the surface (rare gas or condensed molecules) (Refs. 25–28) also received considerable attention. Image states, in which an electron is trapped in the long-range image charge potential and travels in front of the surface, are the delocalized equivalent of the transient negative-ion states that are localized on an adsorbate. Their characteristics (energy and lifetime) are quite sensitive to the surface environment. Theoretical studies of this problem have been developed by modeling the electrostatic potential modifications introduced by the presence of an insulator layer on the metal surface.[26,28] Finally, one should mention studies of negative-ion formation by electron impact on a molecular layer adsorbed on a metal surface and covered by an insulating overlayer,[29] which also imply modifications of transient state characteristics due to an insulating environment. The survival of these negative ions during their escape from the surface has been studied using an electrostatic modeling of the insulator layer effect,[30] and the corresponding predictions have been successfully compared to the experimental data.

In the past, we have extensively studied the excitation and reactive processes induced by electron impact on condensed gases.[1,2] In particular, we can mention the case of a thick film of N_2 condensed on a metal substrate.[31–33] RGS matrix films have been used to dilute the reactive medium, formed by different condensed species. RGS films of variable thickness have also been employed as mere spacers to study the long-range interaction between the metal substrate and condensed molecules.[34] However, this is not the only possible effect since the RGS film may also modify the electronic environment of the molecule. This has been convincingly shown in Ref. 34 where the $v=1$ excitation function, measured around the $^2\Pi_g$ resonance energy for 0.1 monolayer (ML) of N_2 physisorbed on an Ar film of variable thickness (i.e., 0–32 ML) condensed on a Pt substrate is presented. At large thicknesses, the boomerang structure is perfectly visible, but is significantly different from that observed in the gas phase. This is clearly observed[34] even for a 32-ML Ar film, for which the N_2 molecule is located at about 100 Å from the metal surface. Besides, the excitation function exhibits a downward energy shift, which increases when the thickness of the RGS film is reduced. This is not surprising since, when the N_2^- compound state is formed closer to the metal, the attractive image charge potential is stronger. The boomerang structure fades away, however, when the molecule is adsorbed on the bare metal substrate and in the case of the monolayer and bilayer.

The present work is devoted to a joint experimental and theoretical study of the electron impact vibrational excitation of N_2 molecules adsorbed on RGS films condensed on a metal surface so as to explain more adequately these previous results. The latter are now extended to the $v=2$ and 3 decay channels. Furthermore, we discuss modifications of the dynamics of the N_2 vibrational excitation process and in particular of the ''boomerang'' oscillations associated with the N_2^- ($^2\Pi_g$) resonance as a function of the thickness of the underlying insulating film. In this way, we can characterize the effect of the environment on the resonance characteristics. In addition to modifications due to the space asymmetry introduced by the insulating surface, the main result is a stabilization of the N_2^- transient state in front of the RGS spacer. These two effects account well for the intriguing features observed experimentally in the boomerang structure of the excitation functions.

II. EXPERIMENT

The electron-scattering measurements were performed with a hemispherical electrostatic electron energy loss (EEL) spectrometer[31] having the following characteristics. With polar coordinates defined relatively to the outward normal of the sample, the polar angle of the monochromator (i.e., the angle of incidence, θ_0) can be rotated between 14° and 70° at a fixed azimuthal angle. The polar angle of the analyzer (i.e., the angle of analysis, θ_d) is fixed at 45° at the opposite azimuth. Double-zoom electron lenses mounted at the exit of the monochromator and also at the entrance of the analyzer allow the focusing of the incident and analyzed electron beam on the sample over a wide energy range (e.g., 1–20 eV). An EEL spectrum is obtained by fixing the energy of the monochromator while sweeping the energy of the analyzer. The incident electron energy dependence of a given energy-loss feature, also termed the excitation function, is obtained by sweeping the energy of both the monochromator and analyzer while keeping a difference between their energy equal to the probed energy loss. The EEL spectrometer is housed in a bakeable cryopumped ultrahigh-vacuum system (UHV)[34]

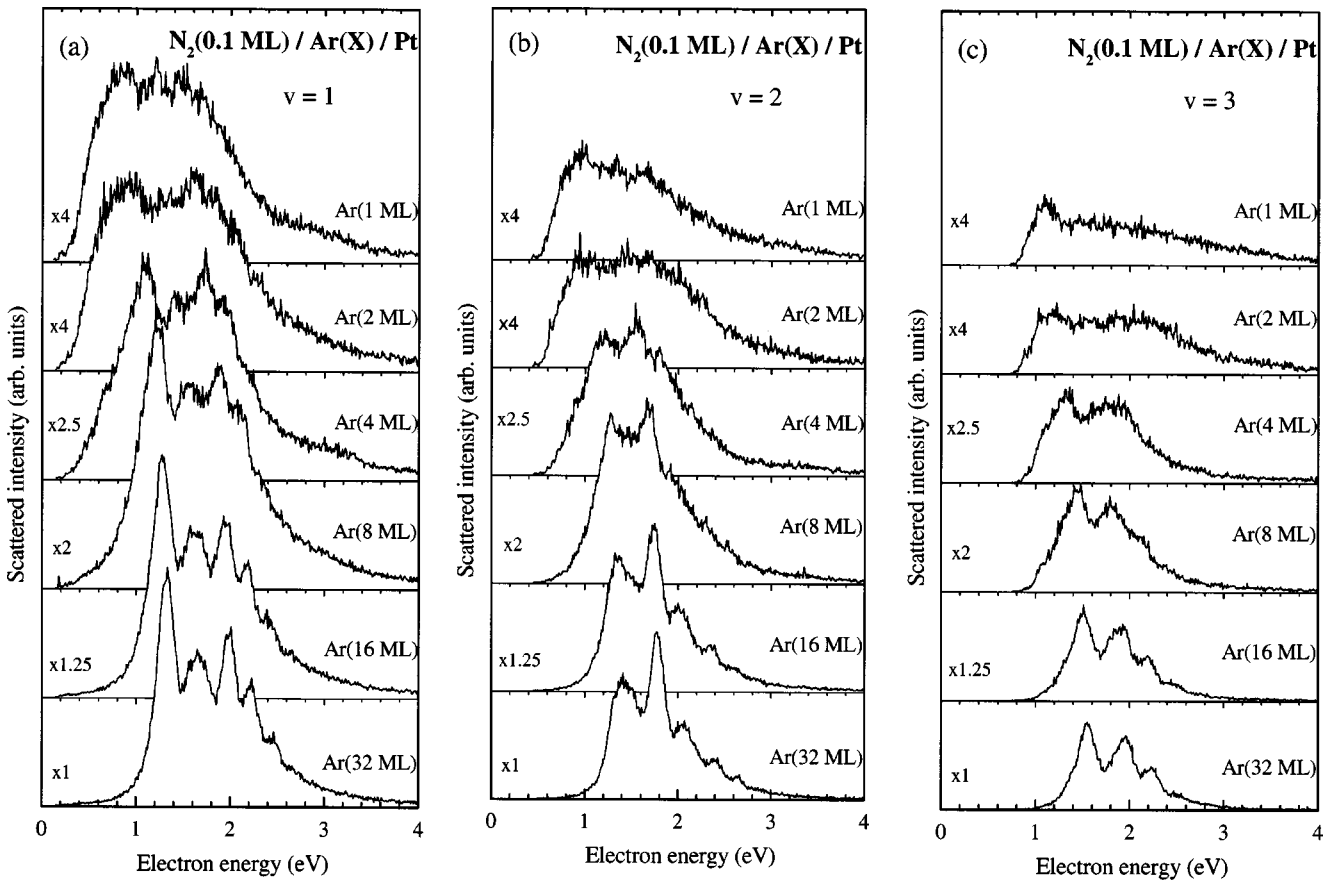

FIG. 1. $^2\Pi_g$ resonance-excitation functions for the $v=1,2,3$ vibrational levels of 0.1 ML of N_2 physisorbed on a solid Ar film whose thickness is increased from 1 to 32 ML. The angle of incidence, θ_0, is 14° and that of analysis, θ_d, is 45°.

at a typical base pressure of 5×10^{-11} Torr. The samples to be studied are condensed from gas phases onto a metal substrate cooled at 14 K. The gases initially prepared in a gas-handling manifold are introduced in the system through a valve which is connected to a small tube having an opening located in front of the metal substrate. This latter is electrically isolated and press fitted with a ceramic plate to the tip of the cryopump which is mounted on a bellows to allow for *X, Y, Z* positioning. The gas-handling manifold consists of two different gas sources connected to a small calibrated volume through bypass and precision-leak valves. In the present experiment, the combined resolution of the selectors was adjusted at 18 meV full width at half maximum (FWHM) for a corresponding current at the substrate of 0.3 nA. For all the results to be shown in the next section, the incident electron energy (E_0) scale was calibrated with respect to the vacuum level by measuring, within ±0.01 eV, the threshold of the electron current transmitted through the deposited films (i.e., current measured on the substrate).

The metal substrate consists of a $2.0\times1.0\,\mathrm{cm}^2$ polycrystalline platinum (Pt) ribbon of 0.2 mm nominal thickness supplied by the Ventron Corporation with a stated purity of 99.95%. The ribbon was cleaned by resistive heating in UHV to a temperature of 1500 °C and, in the presence of oxygen, to 900 °C. The EEL spectra obtained after these treatments were free from any spurious vibrational losses. The metal surface could be further characterized from the observation of low-energy electron diffraction (LEED) threshold interference structures present in the energy dependence of the intensity of the electron beam reflected specularly (i.e., 00 beam). This analysis indicated the presence of disordered Pt microcrystals with a large number of microfacets having the (111) plane parallel to the surface with a strong azimuthal disorder. Ar and N_2 gases were supplied by Matheson of Canada Ltd., both with a stated purity of 99.9995%. The amount of gas leaked into the vacuum system was monitored by the differential pressure drop in the gas-handling manifold. The number of condensed monolayers was estimated to $\pm10\%$ from the calibrated amount of gas needed to deposit one monolayer, assuming no change of the sticking coefficient for the adlayers, as previously described.[35,36] We found, from the observation of the amplitude of the quantum-size interferences in the transmitted as well as reflected current in the specular direction, that Ar film grow layer by layer up to eight monolayers in an azimuthally disordered fcc polycrystal with a preferential (111) orientation normal to the surface and with a minimal addition of defects in going up to 50 ML.[35]

III. RESULTS

In Figs. 1(a), 1(b), and 1(c) we present the $^2\Pi_g$ resonance-excitation functions for the $v=1$, 2, and 3 vibrational levels of 0.1 ML of N_2 physisorbed on an Ar spacer,

TABLE I. Overtone excitation ratio as a function of the Ar film thickness.

Rare-gas film thickness (ML)	$\frac{\int\sigma(0\to2)dE}{\int\sigma(0\to1)dE}$		$\frac{\int\sigma(0\to3)dE}{\int\sigma(0\to2)dE}$	
	Theory	Experiment	Theory	Experiment
0	0.22		0.27	
1	0.40	0.50 ± 0.04	0.40	0.54 ± 0.04
2		0.55 ± 0.04		0.55 ± 0.04
4	0.45	0.56 ± 0.04	0.46	0.55 ± 0.05
8	0.47	0.55 ± 0.04	0.49	0.51 ± 0.04
16	0.48	0.56 ± 0.04	0.52	0.51 ± 0.04
32		0.55 ± 0.04		0.52 ± 0.04
Free molecule	0.50	0.50[a]	0.57	0.69[b]
		0.47[b]		

[a]From Ref. 38.
[b]From Ref. 39.

the thickness of which is increased from 1 to 32 ML. The angle of incidence, θ_0, is 14° and that of analysis, θ_d, is 45°. The boomerang structures present in the three vibrational levels are different from those in the gas phase (see, e.g., Refs. 16 and 37–39) as well as on the bare metal substrate (shown in Fig. 1 of Ref. 33). A striking feature is the drop of the second peak in the boomerang structure of the $v=1$. The strong modifications, which are observed even away from the metal, indicate that N_2 adsorbed on a thick rare gas slab experiences a potential quite different from that felt in the free molecule. The overtone excitation ratio, which is defined as the ratio between the $v=1$, 2, and 3 excitation functions integrated over the collision energy, is given in Table I as a function of the Ar film thickness. For large film thicknesses, the overtone ratio is virtually constant, thus showing that a convergence of the excitation has been reached. We further note that this limit is close to the value for the free molecule, although the shape of the boomerang structure is different. The same is not true for N_2 molecules physisorbed on a clean metal surface, where it has been shown, both experimentally and theoretically, that the overtone excitation ratio is considerably reduced compared to the free-molecule case.[12,16] This effect has been attributed to both a reduction in the resonance lifetime and the space asymmetry due to the presence of the metal surface.[16]

IV. THEORETICAL METHOD

The theoretical description is based on the coupled angular mode (CAM) method, a formulation developed to handle resonant electron scattering by molecules located in an anisotropic environment.[16,40,41] The electron is scattered by the combined molecule-surface system. When molecular adsorption does not perturb too much the electronic properties of the adsorbate and substrate, as in the case of physisorption, the electron-molecule, $V_{e\text{-mol}}$, and the electron-substrate, $V_{e\text{-}S}$, interactions can be considered additive and the Hamiltonian for the electron can be written as

$$H=T+V=T+V_{e\text{-mol}}+V_{e\text{-}S}, \tag{1}$$

where T is the electron kinetic energy. Up to now this method has been used to treat free molecules or molecules physisorbed on free-electron metal surfaces.[16,40,41] In the present case, the electron-substrate interaction includes the interaction with the rare-gas film and the underlying metal substrate.

A. Electron-substrate interaction potential

The present system consists of a single molecule physisorbed on top of a RGS film deposited on the surface of a metal. We mainly consider Ar films of variable thickness. Some results for Xe films are also shown to further illustrate the interpretation of the effect of the RGS film. The rare gases grow on metal surfaces in a fcc structure in the (111) direction. The atomic planes are spaced by a distance $l_{\mathrm{Ar}}=3.04$ Å ($l_{\mathrm{Xe}}=3.58$ Å) in the (111) direction. The interface plane is located half a monolayer spacing from the outermost atomic plane. So the thickness t of a rare-gas film is equal to n times l_{Ar} (or l_{Xe}), where n is the number of monolayers of rare gases.

The free-electron metal substrate is described in the jellium approximation. The electron interaction with the combined system of RGS film and metal substrate is described by classical electrostatics, treating the film as a dielectric continuous medium (DCM).[42] The shape of the potential is very close to that used by Hotzel *et al.*[28] The DCM is characterized by two constants: the dielectric constant ε and the bulk electron affinity (EA). The latter corresponds to the bottom of the conduction band of the bulk dielectric. Depending on the RGS, the bottom of the conduction band is located either below the vacuum level (EA$=0.45$ eV for Xe) or above the vacuum level (EA$=-0.25$ eV for Ar).[43] The ε dielectric constant ($\varepsilon=1.7$ for Ar and 2.2 for Xe) has been obtained from the Clausius-Mossotti relation using the atomic polarizability and the volumes of the primitive cells.[43,44]

The electron in front of the metal surface covered by a dielectric slab of thickness t feels a modified image charge potential. The polarization interaction induced by the negative charge is screened by the dielectric slab depending on its dielectric constant ε. In this problem, there are two interfaces that separate three different regions of space: the metal substrate ($z<0$), the dielectric medium ($0<z<t$), and vacuum ($z>t$). The z electron coordinate is defined with respect to the metal image plane ($z=0$). The potential energy of an electron in the various regions is given by

$$V_{e\text{-}S}(z)=-\frac{e^2}{4\varepsilon}\left(\sum_{k=1}^{\infty}\frac{(-\beta)^k}{kt-z}+\sum_{k=0}^{\infty}\frac{(-\beta)^k}{kt+z}+\frac{2\ln(1+\beta)}{t}\right)-EA, \quad \text{for } 0<z<t, \tag{2}$$

$$V_{e\text{-}S}(z)=-\frac{e^2}{4}\left(\frac{\beta}{z-t}+\frac{4\varepsilon}{(\varepsilon+1)^2}\sum_{k=0}^{\infty}\frac{(-\beta)^k}{kt+z}\right), \quad \text{for } z>t, \tag{3}$$

with $\beta=(\varepsilon-1)/(\varepsilon+1)$; and

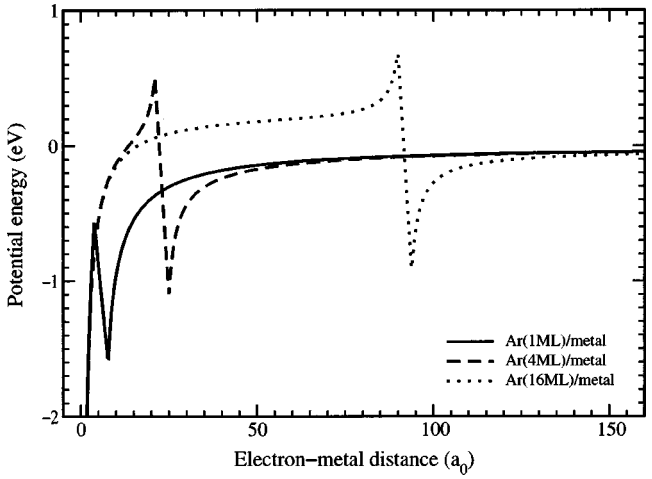

FIG. 2. Electrostatic potential along the normal to the surface for three different Ar film thicknesses in the continuous dielectric model: 1 ML (solid line), 4 ML (long dashed line), and 16 ML (dotted line). The origin of coordinates is the metal image plane.

$$V_{e\text{-}S}(z) = -V_0/(1+Ae^{Bz}), \quad \text{for } z<0. \tag{4}$$

The potential inside the metal, Eq. (4), has the form proposed by Jennings *et al.*[45] The values of the A and B parameters are defined from the jellium parameters λ and V_0 by assuming the continuity of the potential and its derivative at the bare metal surface. In the present case, we have chosen $\lambda = 0.97 a_0^{-1}$ and $V_0 = 13.74$ eV. The corresponding potential in vacuum (i.e., with no dielectric slab) would be given by

$$V(z) = -\frac{1}{4z}(1-e^{\lambda z}).$$

At metal- and vacuum-film interfaces, the electrostatic potential presents a discontinuity. Various methods have been proposed to remove these divergences.[26,28,30] In the present work, at the metal-film interface, the potential is chosen to be constant and equal to $-\lambda/4$; it thus joins the relation (4) at $z=0$ and Eq. (2) inside the dielectric. At the vacuum-film interface, we use the recent prescription of Hotzel *et al.*[28] who introduce a linear variation of the potential between $t-b/2$ and $t+b/2$ to remove the divergence at t. The distance b is related to the energy jump $-EA+E_p$, with E_p the polarization energy induced by a point charge in the bulk medium of the dielectric constant ε:

$$b = \frac{\varepsilon-1}{\varepsilon}\frac{e^2}{2E_p}. \tag{5}$$

For Ar, the polarization energies found in the literature[46] lie between 1 and 1.4 eV, which corresponds to b values between 2.11 and 2.96 Å. In our calculation, we have chosen $b_{\mathrm{Ar}} = 2.11$ Å. In the case of Xe, $b_{\mathrm{Xe}} = 2.73$ Å according to Ref. 28.

Figure 2 presents the electron-substrate interaction potential in the case of Ar slabs of 1, 4, and 16 ML thickness. For a sufficiently thick film (e.g., 16 ML), the potential is relatively flat inside the RGS film and its value corresponds to the bottom of the conduction band of the bulk dielectric. The potential presents a steep variation near the vacuum-film interface. It appears that this interface effect dominates the potential at small thickness. Because of the importance of the interface region, the DCM should be used with care in the case of thin films. Below, we present results for various thicknesses, but the details are concentrated on the results for thick films.

B. Electron-molecule interaction:

The electron-molecule interaction is modeled by the effective range theory (ERT) approximation.[47,48] In this method, the electron space around the molecule is cut into two regions. In the outer region ($r>r_c$), where r is the electron-molecule distance, the electron-molecule interaction is described explicitly via a long-range interaction potential and one assumes the separation of angular modes, which are taken as spherical harmonics Y_{lm} in the present case of N_2. The long-range interaction potential is taken from the *ab initio* study of Le Dourneuf *et al.*[49] The effect of the short-range interaction region ($r<r_c$) is treated via a boundary condition on the electron radial wave function F_{lm} at the boundary $r=r_c$:

$$\frac{1}{F_{lm}}\frac{dF_{lm}}{dr}\bigg|_{r=r_C} = f_{lm}. \tag{6}$$

The boundary condition f_{lm} depends on the internuclear distance R of the molecule. In the present work, we followed the same approach as in our previous work on N_2 molecules physisorbed on a metal surface.[10,16] The N_2^- ($^2\Pi_g$) resonance is associated with a $d\pi$ ($l=2$, $m=\pm 1$) wave in the molecular frame. In particular, the ERT modeling of the e-N_2 scattering in the region of the N_2^- ($^2\Pi_g$) resonance quantitatively reproduces the boomerang structure and the overtone ratios in the case of electron scattering by a free molecule and their modification in the case of a molecule physisorbed on a free-electron metal.[16]

C. CAM coupled equations

The essence of the CAM method is to expand the electron wave function $|\Psi\rangle$ over an angular basis that is well adapted to the description of the electron-molecule interaction: the basis of spherical harmonics centered on the molecule. Two types of situations are investigated: electron scattering by a static molecule (fixed internuclear distance R) and electron scattering by a vibrating molecule. For the problem of an electron scattered by a molecule with a fixed internuclear distance, one has

$$|\Psi\rangle = \sum_{lm} \frac{1}{r}F_{lm}(r)|Y_{lm}\rangle, \tag{7}$$

where F_{lm} is the electron radial wave function associated with the lm angular momentum. The electron-substrate interaction, which is not of spherical symmetry, generates coupling terms between the different spherical harmonics $\langle lm|V_{e\text{-}S}|l'm\rangle$. In the case where the N_2 molecular axis is

perpendicular to the surface, the molecular axial symmetry is retained and the expansion (7) has to contain only terms with $m=\pm 1$ to treat the N_2^- ($^2\Pi_g$) resonance. In the case of another orientation of the molecular axis, the symmetry of the problem is lowered, and a few m terms have to be considered (see the discussion in Ref. 50), leading to the splitting of the N_2^- ($^2\Pi_g$) state into two resonances. Below, we present results for two geometries—molecular axis parallel or perpendicular to the surface—in order to discuss the effect of the adsorption geometry. As shown in Ref. 50, for the parallel geometry, the N_2^- ($^2\Pi_g$) state splits into two resonances with different characteristics: symmetric or antisymmetric with respect to a plane normal to the surface and containing the molecular axis. The symmetric resonance characteristics (parallel geometry) are very close to those of the doubly degenerate resonance in the perpendicular geometry, whereas the asymmetric one is different, being less perturbed by the presence of the surface. The presentation of the theoretical approach below is done for the perpendicular geometry: the modifications required to treat the parallel geometry case can be found in Ref. 50.

For electron scattering from a fixed-nuclei molecule at energy E, bringing the expansion (7) into the Schrödinger equation yields a set of coupled radial equations (in the perpendicular geometry, m is a good quantum number equal to $+1$ or -1):

$$-\frac{1}{2}\frac{d^2F_{lm}(r)}{dr^2}+V^{lm}_{e\text{-mol}}(r)F_{lm}(r)+\sum_{l'}\langle lm|V_{e\text{-}S}|l'm\rangle F_{l'm} =EF_{lm}(r), \tag{8}$$

the F_{lm} radial wave functions verifying the boundary condition (6). The coupling introduced by the electron-substrate interaction does not vanish at infinity and so, after solving the above equations in the spherical harmonics basis, one has to perform a basis change into the angular basis that diagonalizes the interaction at infinity (adiabatic angular modes). The scattering S matrix can be extracted in this adiabatic angular basis. The analysis of the energy dependence of the corresponding time delay matrix[51] then yields the energy position and width of the N_2^- resonance perturbed by the surface. Indeed, these energies and widths depend on the molecule internuclear distance.

To study the electron impact vibrational excitation process, one has to describe the electron scattering and molecular vibration at the same time, since the resonance lifetime is of the order of magnitude of the vibrational frequency. The CAM procedure allows treating this problem exactly within the ERT approximation. The total wave function of the system is expanded over the angular basis set *and* over a nuclear basis set; the nuclear basis set is the basis of vibrational wave functions of the neutral N_2 molecule. One thus has

$$|\Psi\rangle=\sum_v\sum_l\frac{1}{r}F^v_{lm}(r)\chi_v(R)|Y_{lm}\rangle. \tag{9}$$

The boundary condition at $r=r_C$ on the radial wave functions is now written as

$$\sum_v\left\{\left.\frac{dF^v_{lm}}{dr}\right|_{r=r_C}\delta_{v'v}-\langle\chi_{v'}|f_{lm}(R)|\chi_v\rangle F^v_{lm}(r_C)\right\}=0. \tag{10}$$

Bringing the expansion (9) into the Schrödinger equation leads to a set of coupled equations for the radial wave functions $F^v_{lm}(r)$. Couplings only exist inside each block v, and the coupled equations are analogous to Eq. (8). Their solution in the spherical harmonics angular basis followed by the transformation into the adiabatic angular mode basis yields the scattering S matrix in the (v,i) basis product of the N_2 vibrational basis and of the adiabatic angular mode basis.

D. Vibrational excitation probabilities and cross sections

The solution of the CAM coupled equations yields the scattering S-matrix elements $S_{v_fk',v_ik}(E)$, which connect the initial state v_i,k (vibrational level v_i, adiabatic angular mode k) to the final v_f,k' state (vibrational level v_f, adiabatic angular mode k'). They depend on the incident collision energy E. By analogy with the case of scattering by a free molecule, one can define the inelasticity $I_{vi\to vf}$ for the vibrational transition from the initial vibrational level v_i to the final level v_f:

$$I_{v_i\to v_f}(E)=\sum_{k,k'}|S_{v_fk',v_ik}(E)|^2. \tag{11}$$

The inelasticities play the role of vibrational excitation probabilities; for a free molecule, they are directly proportional to the total excitation cross sections for the various vibrational transitions.

In the presence of the substrate-vacuum interface, the electron space is divided into two regions, the vacuum side and the substrate side, with different asymptotic energies and so different vibrational excitation properties. In an electron-induced excitation process, one can then define four different processes, depending on the regions of space where the incident electron is coming from and where the outgoing electron is going to (see the discussion in Ref. 16). For example, a ''usual'' scattering experiment will correspond to scattering from and to the vacuum (VV process). But other processes involving the metal or substrate side (M) are also present and important; they involve hot electrons in the substrate. In principle, the adiabatic angular modes belong either to the (M) or (V) side.

In our previous studies,[16] which involved a free-electron–metal–vacuum interface, the separation between V and M adiabatic modes was not fully converged for the finite angular basis used. Instead, we had taken an alternative and efficient method that consists in sharing the excitation probability between the M and V sides, according to a classical description of the electron refraction by the long-range image charge potential.[16] In the present case, the strong variation of the electrostatic potential at the substrate-vacuum interface introduces a very efficient effective separation of the adiabatic angular modes. This separation converges with a rather limited size of the angular basis and allows recognizing the adiabatic angular modes belonging to the V or metal

M sides. Thus we can define the vibrational excitation probabilities for the various processes (*VV*, *VM*, *MV*, or *MM*) by restricting the sum in Eq. (11) to the relevant adiabatic angular modes. From these, we can define the ''summed'' excitation cross sections that are defined as the integrals of the differential excitation cross section over the final angle, averaged over the initial angle, the initial and final angle variation being restricted inside *M* or *V*. One thus has for the *VV* summed cross section, to be compared with scattering experiment results,

$$\sigma_{VV}(v_i \rightarrow v_f) = 2\pi \sum_{k,k' \in V} \frac{1}{k_i^2} |S_{v_f k', v_i k}|^2, \qquad (12)$$

where the sum over the angular modes is restricted to the ones belonging to the *V* side. k_i is the electron momentum in the incident channel. Analogous expressions are obtained for the *VM*, *MV*, and *MM* processes. The factor of 2 in Eq. (12) is associated with the double degeneracy of the N_2^- ($^2\Pi_g$) resonance in the perpendicular geometry. In the parallel geometry, the two contributions from the two resonances have to be summed.

The following basis set was found to be sufficiently large to reach convergence in the present problem: we used 12 spherical harmonics for the electron angular basis and 14 vibrational levels for the nuclear basis. The size of the system of coupled equations was thus 12×14. Their solution, using the De Vogelaere propagator,[52] was performed in a sphere of radius of $(300-600)a_0$ depending on the RGS film thickness.

V. N_2 PHYSISORBED ON Ar FILMS: N_2^- ($^2\Pi_g$) RESONANCE ENERGY POSITION AND WIDTH

The static properties of the N_2^- ($^2\Pi_g$) resonance (energy position and width) are consistently extracted from a calculation with a fixed-nuclei molecule. The coupling of a negative-ion state with the electronic continuum of the substrate strongly depends on the normal distance of the molecule to the film-vacuum interface (i.e., adsorption height), *Z*. To modify the strength of the coupling, we can vary this distance *Z*. The adsorption height in the N_2/Ar/metal-physisorbed system has been estimated from the equilibrium distance (3.9 Å) of the N_2-Ar van der Waals molecule.[53] Assuming that the Ar film surface corresponds to a fcc (111) plane, we computed the N_2 equilibrium adsorption height for the hollow, bridge, and top sites, to be $3.3a_0$, $3.6a_0$, and $4.5a_0$ from the image plane, respectively. Below, we use the hollow site value; the results for the bridge site distance configuration should be very similar.

Figure 3 presents the energy shift and width of the N_2^- ($^2\Pi_g$) resonance as function of the N_2 adsorption height *Z* on a 4-ML Ar film. The N_2 internuclear distance is at equilibrium. Figure 3 presents the results for the doubly degenerate resonance in the perpendicular geometry and for the antisymmetric resonance in the parallel geometry (the symmetric resonance in this case is extremely close to the perpendicular geometry case and is not shown here). At large *Z*, the resonance energy and width correspond to those of the free-molecule values (i.e., 2.3 and 0.4 eV, respectively). The resonance energy shifts with the molecule-surface distance, roughly following the electron-substrate interaction potential [dashed line in Fig. 3(a)]. In the perpendicular geometry, this downward energy shift stops around $3.0a_0$, i.e., in the vicinity of the estimated adsorption height. For smaller distances, an increase of the energy of the resonance follows the shape of the interaction potential, which presents a steep repulsive wall near the interface (Fig. 2).

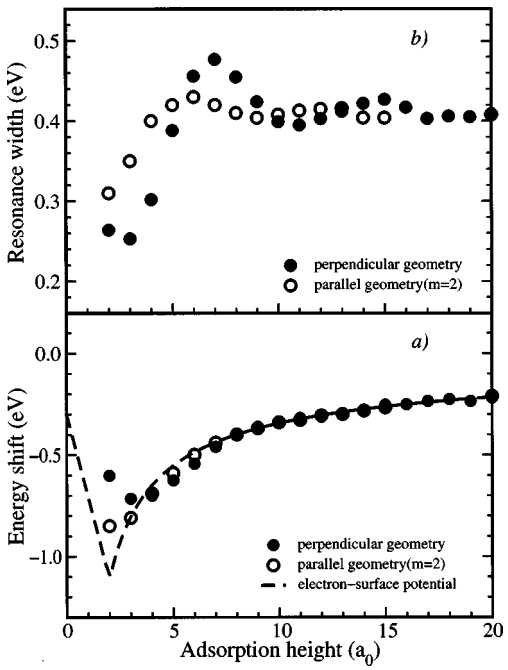

FIG. 3. a and b N_2^- ($^2\Pi_g$) resonance energy shift (a) and width (b) (in eV) as a function of the adsorption height (in atomic units, measured from the film-vacuum interface). The resonance energy shift (a) corresponds to the difference in energy position of the resonance between an adsorbed molecule and the free molecule. This shift is compared with the electrostatic potential along the surface normal (dashed line). The Ar film thickness is 4 ML. Solid circles: molecular axis perpendicular to the surface ($m=1$). Open circles: antisymmetric resonance ($m=2$) for the molecular axis parallel to the surface.

In Fig. 3(b), the width of the resonance energy presents small oscillations, which increase in amplitude as the molecule approaches the surface. Thus the resonance may either be longer lived or shorter lived than in free space, depending on *Z*. These oscillations are due to the steep potential variation around the film-vacuum interface (see Fig. 2), which acts as a partially reflecting barrier. This generates interference between the molecular resonance wave function and the escaping electron wave that is reflected at the interface. The period of the oscillations as a function of *Z* is consistent with this interpretation.

Similar oscillations have been found in previous studies on molecules adsorbed on a metal surface where a steep potential variation is present or when the surface is reflective due to the electronic band structure.[8,17,54] This interference effect either increases the resonance decay or partially blocks it. As a result, at the estimated actual adsorption height *Z*

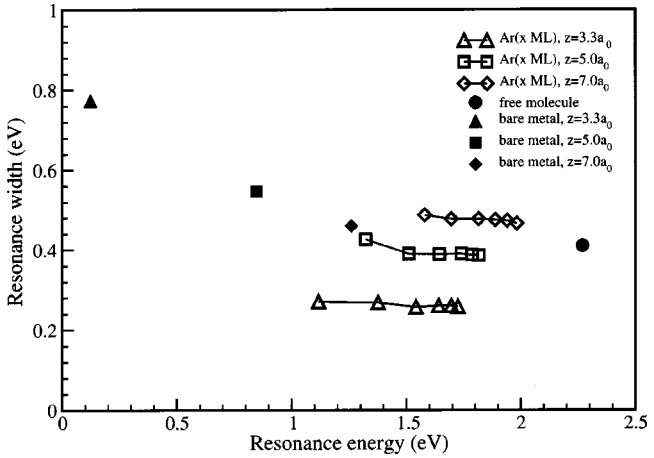

FIG. 4. Width of the N_2^- ($^2\Pi_g$) resonance vs its energy position, for three different adsorption heights Z (3.3, 5.0, and 7.0 a.u. measured from the film-vacuum interface: triangles, squares, and diamonds respectively). The open symbols correspond to an Ar film of variable thickness (1, 2, 4, 8, 16, and 32 ML). The solid symbols correspond to the case of a bare metal with the same adsorption height. The solid circle gives the free-molecule result.

$=3.3a_0$, the resonant state has a much longer lifetime than in free space. The presence of the insulating film thus results in the stabilization of the transient negative ion.

The results for the antisymmetric state (parallel geometry) exhibit the same qualitative features as in the perpendicular geometry; however, they slightly differ quantitatively. As explained in Ref. 50, the difference can be linked to the shape of the $d\pi$ resonant orbital. In a perturbation picture, the ''cloverleaf'' shape of the orbital leads to different interactions, depending on whether the cloverleaf is perpendicular or parallel to the surface. The latter case (antisymmetric resonance in the parallel geometry) leads to a weaker interaction with the surface and thus to a smaller perturbation. This accounts well for the smaller amplitude of the width oscillations in Fig. 3(b) and to a resonance energy that is closer to the potential at the molecule center in Fig. 3(a). At the adsorption height, the antisymmetric resonance (parallel geometry) thus appears to be slightly lower in energy and broader than the resonance in the perpendicular geometry.

We further studied the influence of the RGS film thickness on the static properties of the resonance for three different adsorption heights: $3.3a_0$, which corresponds to the estimated N_2 adsorption height, $5.0a_0$, where the width is roughly equal to the value in the free molecule, and $7.0a_0$, where the resonance is less stable than in the free molecule. In Fig. 4, we present the resonance width as a function of the resonance energy in the perpendicular geometry for different Ar film thicknesses (open symbols for 1, 2, 4, 8, 16, and 32 ML; the order of the points follows that of the thicknesses, the smallest thickness corresponding to the lowest resonance energy). Also included is the case of the free molecule and that of a molecule directly physisorbed on the bare metal surface at the same molecule-surface distance (solid symbols). It must be stressed here that the adsorption height is different on a bare metal from on an Ar film. In our earlier work,[16] it was estimated to lie around $5a_0$ from the image plane.

For a given distance between the molecule and film surface, decreasing the rare-gas film thickness leads to a decrease of the resonance energy. This is not surprising since, in a first approximation, the resonance energy shift is given by the electron-substrate interaction potential at the center of the molecule. The formation of a negative-ion state near the surface of the metal induces polarization charges that appear at the metal–dielectric-film interface. However, this polarization charge is partially screened by the dielectric medium due to its finite dielectric constant. In addition, the effect of the metal interface decreases when the distance of the molecule to the metal surface increases, i.e., when the film thickness increases (see Fig. 2). This accounts for the variation of the resonance position with film thickness and Z.

On the other hand, the resonance width, which strongly depends on the distance between the molecule and film surface, is nearly independent of the dielectric film thickness from 1 to 32 ML (the case of a bare metal appears to be different). This effect shows up as three different plateaus in the resonance width versus the energy position. The same type of oscillations as observed for a 4-ML film in the resonance width as a function of Z [Fig. 3(b)] is present for all dielectric film thicknesses. This is consistent with the above interpretation involving the reflectivity of the vacuum-dielectric interface as the key parameter for the resonance width.

The case of an N_2 molecule adsorbed on a dielectric film is definitively different from the case of a molecule directly adsorbed on a bare free-electron metal surface.[8–10] In the latter case, one obtains a large downward energy shift of the resonance (roughly given by the $-1/4Z$ term, coming from the image charge attractive potential), associated with a steady increase of the width. The resonance becomes more unstable when the molecule is adsorbed on a free-electron metal substrate. It is clear from Fig. 4 that this situation is completely modified when the molecule is adsorbed on a dielectric film, whatever its thickness. Differences in the resonance energy position are connected to differences in the electron-surface interaction potential at the center of the molecule, whereas the peculiarities of the resonance width for the Ar film are connected to the existence of a steep potential variation at the vacuum-dielectric interface.

The same kind of behavior is obtained for a Xe dielectric spacer. Figure 5 presents a comparison of the N_2^- ($^2\Pi_g$) resonance width at the N_2 equilibrium internuclear distance as a function of Z, in the case of 4-ML films of Ar or Xe. As a striking feature, the oscillations of the resonance width as a function of Z are quite similar, while the amplitude is larger for the Ar film. Again, this is consistent with the interpretation in terms of the reflectivity of the vacuum-dielectric interface; the period of the oscillations depends only on the geometry and resonance energy, which is almost the same in the two cases. The reflectivities of the two surface barriers are slightly different for Xe and Ar films. The two rare-gas systems differ in particular by the energy of the bottom of the conduction band, which lies above the vacuum level for bulk Ar and below for Xe. This makes the Ar film more reflecting

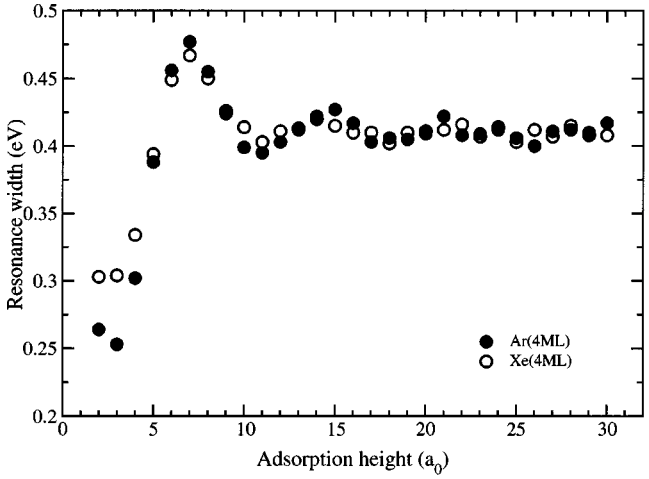

FIG. 5. Comparison between the N_2^- ($^2\Pi_g$) resonance width in the case of 4-ML Ar (solid circles) and 4-ML Xe (open circles) films. The molecular axis is perpendicular to the surface. The widths are presented as functions of the adsorption height, measured from the film-vacuum interface.

and thus accounts for the slight difference in amplitude of the oscillations between the two films and, in particular, the smaller width in the case of Ar at the equilibrium adsorption height (i.e., a resonance width of 0.25 eV for Ar compared to 0.3 eV for Xe). Although these effects comes from the surface barriers, we do not expect the exact shape of the potential very near the interface plane and, in particular, the manner in which the discontinuity of the classical electrostatics calculation is treated to be the key parameters. The resonance characteristics should not depend on the way to handle the discontinuity at the dielectric-vacuum interface. For example, assuming a constant potential (equal to the bulk affinity) in the dielectric medium does not modify the resonance characteristics significantly.

VI. THEORETICAL VIBRATIONAL EXCITATION PROBABILITY AND CROSS SECTION

Figure 6 presents the calculated $v=0-1$ excitation probability (i.e., the inelasticity) for N_2 adsorbed in the perpendicular geometry on 1, 4, and 16 ML of Ar as a function of the incident electron energy. The excitation function exhibits an oscillatory structure, which is nearly the same for different Ar film thicknesses, with the exception of a global shift in energy. This feature has to be linked with the results presented in Fig. 4, where the resonance width is shown to be virtually independent of the Ar film thickness, whereas the resonance energy is lowered when the film thickness is decreased. However, this oscillatory structure is clearly different from the one for free N_2 seen at the bottom of Fig. 6. Moreover, the peaks are narrower, more intense, and almost completely separated from each other for N_2 lying on the RGS. The second peak has a much smaller probability than the nearest ones by about a factor of 2, but it is split and broader than the other peaks. This is common to all Ar dielectric films within the present film thickness range. For free N_2, the second peak also exhibits a width broader than

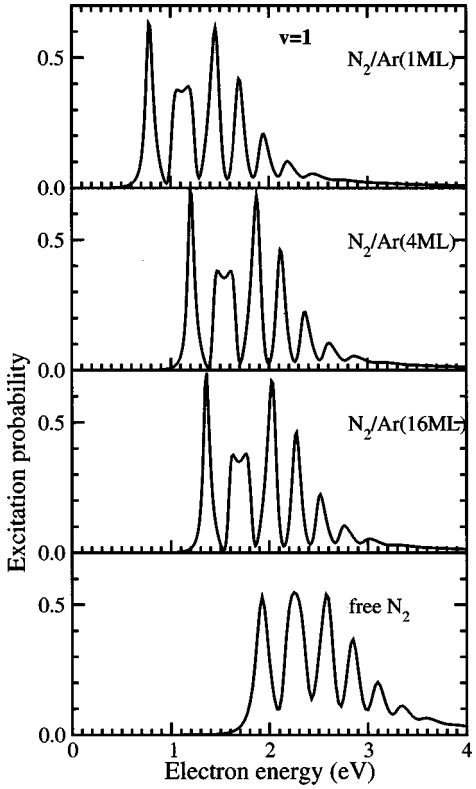

FIG. 6. Vibrational excitation probability ($v=0-1$) as a function of the collision energy, for N_2 molecules adsorbed in the perpendicular geometry on an Ar film (1, 4, and 16 ML). The case of the free molecule is also shown for comparison. The collision energies are measured with respect to the vacuum level.

the other peaks, but with no reduction in intensity.

It is well known that the boomerang structure is highly dependent on the lifetime of the intermediate state.[5,6] In the present case, the resonance lifetime, although longer than in the gas phase, is still comparable to the vibrational period, so that vibrational levels of the intermediate N_2^- ion cannot be defined independently, thus leading to boomerang oscillations. However, the narrowing of the peaks in the excitation function (Fig. 6) is a direct consequence of the decreased total width of the N_2^- ion, due to the presence of the Ar spacer. In the boomerang situation, the peaks cannot be energetically associated with the vibrational levels of the negative-ion intermediate; it must be stressed that the boomerang depends on the vibrational excitation transition that is considered (see below, Fig. 11). Following the arguments given for the free molecule by Herzenberg,[5] the peak interval in the boomerang structure is larger than the vibrational spacing of the N_2^- ion, considered as a stable anion. Thus, if it were possible to go continuously from a boomerang situation to that of a perfectly stable N_2^- ion (i.e., to the long-lifetime limit), one would see an increase of the number of peaks in the vibrational excitation function. In the present study, when going from the free N_2 to N_2 adsorbed on Ar films, the anion's lifetime increases and the splitting of the second peak of the boomerang structure in the $v=1$ vibrational excitation probability function is tentatively attributed to an increase of the number of peaks in the structure asso-

ciated with the transition from the boomerang situation to that of a more stable ion.

Figure 7(a) presents the *VV* cross section for the $v=1$ vibrational excitation for the free molecule and for molecules adsorbed in the perpendicular geometry on Ar films (1, 4, and 16 ML thickness). For the free molecule, the cross section is defined with the same spatial restriction as for the molecules adsorbed on Ar, resulting in a *VV* cross section equal to one-fourth of the total excitation cross section. The cross sections present a boomerang structure similar to that seen in the excitation probability function. As the main feature, the detailed shape and absolute value of the energy dependence of the cross sections depend on the thickness of the Ar film: the cross section is smaller in the 1-ML case than for thicker films. The shape of the barrier at the dielectric-vacuum interface qualitatively explains this effect. The reflectivity of the surface barrier is expected to be higher in the case of a higher and broader barrier. As seen in Fig. 2, the height of the barrier is higher at large film thickness and thus corresponds to a higher reflectivity. The barrier reflectivity influences the resonance lifetime as discussed above, but it also globally increases the scattering into the vacuum, compared to that into the substrate, and this accounts for the film thickness effect observed in Fig. 7(a).

Figure 7(b) presents the results for the parallel geometry. The general discussion of the shape of the *VV* summed cross section and of its thickness dependence is identical to that of Fig. 7(a). The width of the peaks in the boomerang structure appears to be larger than in Fig. 7(a), consistently with the results in Fig. 3(b). Similarly, the second peak in the boomerang structure is not as well resolved as in Fig. 7(a). One can also notice that the decrease of the *VV* cross section when the film thickness decreases is stronger in the parallel geometry than in the perpendicular geometry.

Figure 8 presents the results for the *VV* $v=1$ vibrational excitation summed cross section in the case of N_2 condensed in the perpendicular geometry on a 16-ML film of Xe. The Xe calculations are performed at the same adsorption height as for Ar, although one can expect a larger adsorption height for the Xe case. The comparison with the same molecule-surface distance Z is done to illustrate the effect of the differences in the electrostatic potentials of the Ar and Xe films. These results are very similar to the corresponding ones for a 16-ML Ar film in Fig. 7(a), but the excitation cross section is smaller and the narrowing of the peaks is slightly weaker. These differences between Ar and Xe can be discussed following the above discussion on the fixed internuclear separation results, involving the reflectivity of the dielectric-vacuum interface. Two parameters influence the excitation cross sections: the reflectivity and lifetime of the resonance. In the case of Xe, they both contribute to decrease the *VV* cross sections. The reflectivity of the Xe films is lower than that of the Ar films, owing to the lower conduction band edge in Xe. This lower reflectivity increases the importance of the electron emission towards the substrate and thus decreases emission channels towards vacuum. The shorter lifetime for N_2^- formed on Xe also decreases the magnitude of the excitation. As for the width of the peaks in the excitation function, they are directly connected to the resonance life-

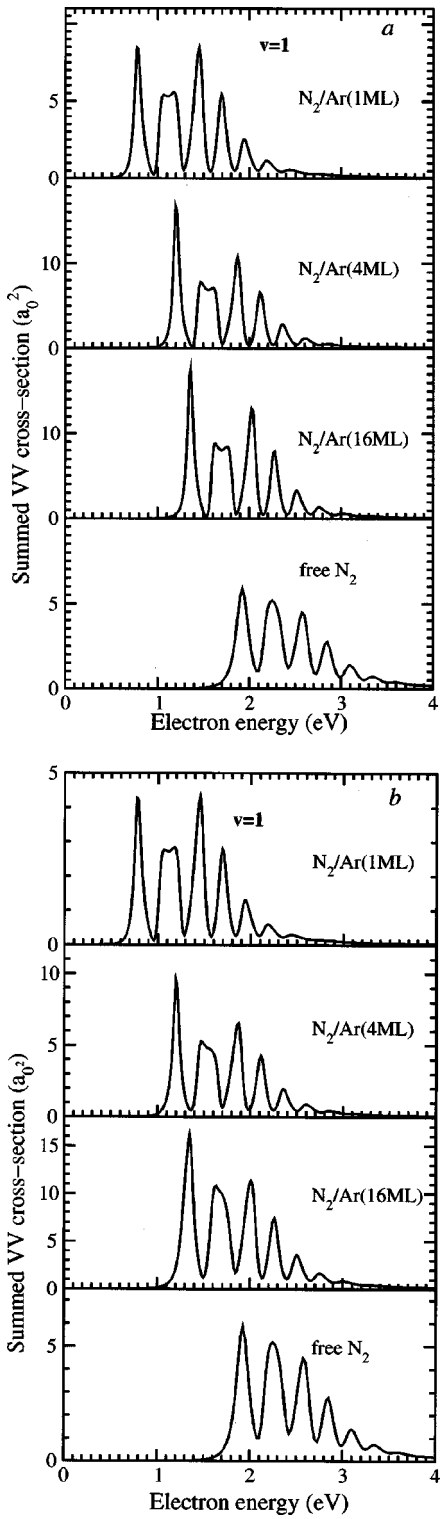

FIG. 7. (a) *VV* summed vibrational excitation cross section ($v=0-1$) as a function of the electron energy, for N_2 molecules adsorbed on an Ar film (1, 4, and 16 ML). The case of the free molecule is also shown for comparison. The molecular axis is perpendicular to the surface. (b) Same as (a) for the molecular axis parallel to the surface.

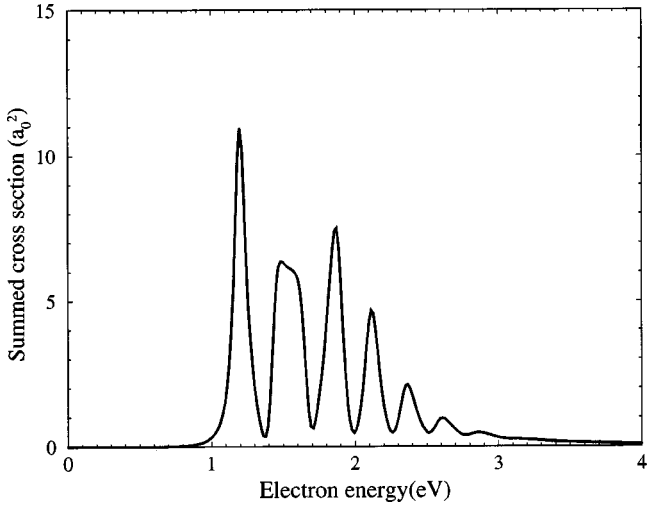

FIG. 8. *VV* summed vibrational excitation cross section ($v=0-1$) as a function of electron energy, for N_2 molecules adsorbed in the perpendicular geometry on a 16-ML Xe film.

time, which accounts for the small difference between the Ar and Xe calculations [Figs. 7(a) and 8].

Figure 9 presents the $v=1$ vibrational excitation cross sections for the four processes *VV*, *VM*, *MV*, and *MM* in the case of a 16-ML Ar film (perpendicular geometry). The *VM* and *MV* summed cross sections are almost identical. The four cross sections are very similar, except for a dominance of the processes involving the vacuum side (i.e., the *MM* cross section is the smallest), indicating that the sharing of the inelasticity favors electron emergence in vacuum. On the contrary, the case of isolated N_2 leads to four equal cross sections. Moreover, these results are quite different from what was found for a molecule directly adsorbed on a bare free-electron metal.[16] In this case, scattering to and from the metal was predominant, especially for low-energy electrons.

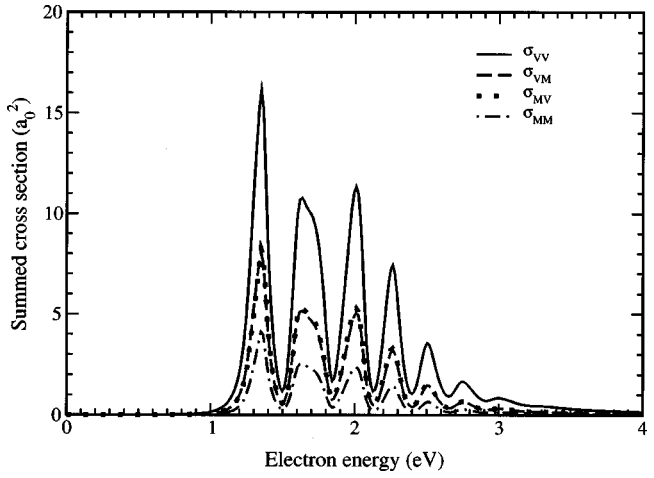

FIG. 9. Comparison between the various *VV*, *VM*, *MV*, and *MM* summed vibrational excitation ($v=0-1$) cross sections as functions of the electron energy for N_2 molecules adsorbed in the perpendicular geometry on a 16-ML Ar film. Solid line: *VV*. Dashed line: *VM*. Dotted line: *MV*. Dashed-dotted line: *MM*. The *VM* and *MV* cross sections are very close to each other.

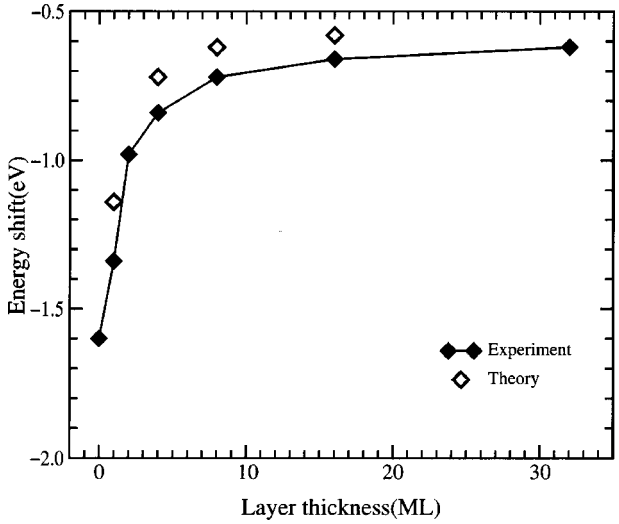

FIG. 10. Comparison between the energy shifts of the N_2 vibrational excitation process ($v=0-1$) obtained in the experimental (solid diamonds) and theoretical studies (open diamonds, parallel geometry).

The difference between the two situations can be interpreted by comparing surface barriers. The surface barrier of a metal is simply the image charge interaction that attracts the electron toward the metal and thus favors strongly electron emission into the metal. In the case of an insulating film, the potential barrier at the vacuum-dielectric interface reflects a larger portion of the electrons back into the vacuum, thus favoring the vacuum side. One can nevertheless notice that this favoring effect in the Ar film case is not very strong compared to the opposite effect in the bare surface case.

VII. DISCUSSION: COMPARISON BETWEEN EXPERIMENTAL AND THEORETICAL RESULTS

A. Energy shift of the vibrational excitation cross section

For a meaningful comparison of the experimental and calculated energy shifts due to the attractive image charge potential, it should be realized that the boomerang interference creates structures in the cross sections that are not the same for different vibrational exit channels. We chose to compare the shift of the energy position of the first peak in the boomerang structure.

As for the adsorption geometry, we do not know what the actual distribution of molecular orientations for the various films is. The difference between the two extreme cases (perpendicular and parallel) is, however, limited [see Figs. 7(a) and 7(b)], in part due to the fact that one of the resonances in the parallel case is identical to that in the perpendicular case. In the following, we use the results of the parallel geometry, which can be expected to have a larger weight than the perpendicular geometry.

Figure 10 presents the excitation cross section energy shift, obtained from the experimental measurements and theoretical calculations, as a function of Ar film thickness. There is a close agreement between these two curves, except for a nearly constant and small energy difference between

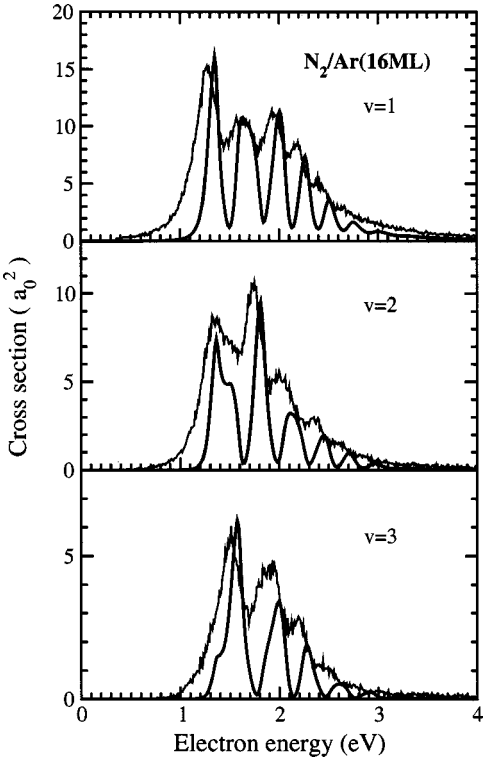

FIG. 11. Comparison between the experimental (thin solid line) and theoretical (thick solid line) vibrational excitation cross sections ($v=0-1$, 2, and 3) as functions of the collision energy for N_2 molecules adsorbed on a 16-ML Ar film.

them. The theoretical shift is smaller than the experimental one by about 0.1 eV between 2 and 16 ML, which is larger than the experimental uncertainty. One can stress that a different choice of molecule-surface orientation would not significantly alter this comparison. It should also be noted that the resonance energy shift reaches its maximum around the equilibrium adsorption height (Fig. 3) and so, within the present choice of electron-substrate interaction potential $V_{e\text{-}S}$ in the DCM model, a better agreement could not be reached merely by changing the adsorption height. A possible reason for this systematic difference then lies in the approximations implied in the present $V_{e\text{-}S}$ potential, especially near the dielectric-vacuum interface.

B. Experimental and theoretical vibrational excitation cross sections

In Fig. 11 the experimental excitation functions for the $v=1,2,3$ vibrational levels of 0.1 ML of N_2 physisorbed on a 16-ML film of Ar are compared to the calculated summed excitation cross sections (parallel geometry). The experimental data are relative values, and only the $v=1$ profile was scaled to the theoretical value (i.e., the ratio between the various curves is meaningful). The comparison in Fig. 11 is between excitation functions at fixed angle and summed cross sections; it makes the implicit assumption that the energy dependence of the excitation cross section is not very sensitive to the scattering angles. This is reasonable for a resonant process, where the angular distributions of the electrons reflects the angular shape of the resonant orbital (here a $d\pi$ orbital perturbed by the surface) and not that of interference phenomena. Nevertheless, a modification of the energy dependence could arise from a combined angular and energy dependence of the reflectivity of the vacuum-dielectric surface barrier.

The measured boomerang structure with all its distinct features in the different vibrational exit channels v (relative positions and intensities) is reproduced rather well by the calculation. The energy shift between the theoretical and experimental boomerang structure (Fig. 10), discussed in the previous section, is also present in the $v=2$ and 3 vibrational exit channels, confirming its systematic character. The structures in the experimental excitation functions are also broader than in the calculated ones. In particular, the experimental $v=1$ cross section extends considerably towards low collision energies. No definitive interpretation of this broadening can be proposed at this time. The energy resolution of the spectrometer (18 meV FWHM) cannot account for this broadening. Besides, a mere convolution of the theoretical data with a correspondingly broad Gaussian profile would not lead to a better agreement. A possibility could be the presence of inhomogeneities in the Ar-N_2 system. One may think of fluctuations in the Ar film thickness, variation in the numbers of neighboring Ar atoms, and the existence of different adsorption sites including interstitial sites.

One could also mention that the resonant intramolecular vibrational excitation of the N_2 molecule should be associated with frustrated rotation and translation of the Ar-N_2 system (i.e., librations and phonons) via a similar resonant process, and this could influence the shape of the energy dependence. It has been found in high-energy electron-energy-loss spectroscopy (HREELS) measurements that the resonant excitation of the intramolecular vibrational excitation was associated with a broadening of the energy-loss peaks toward large energy losses, indicative of an associated unidentified excitation process.[13,55–57] On the theoretical side, it has been shown that the excitation of the molecule-frustrated rotation could be very efficient in the case of resonant scattering.[58]

Since the cross section behavior for all thicknesses above 4 ML, except for a global energy shift, are similar to that seen in Fig. 11, a similar agreement between theory and experiment is reached for all thick films. For smaller Ar coverages, further differences exist between theory and experiment. As seen in Figs. 1(a), 1(b), and 1(c), the boomerang structure gradually disappears as the Ar film thickness goes to zero, while it remains essentially unchanged in the calculations down to 1 ML (see Figs. 6 and 7). Earlier calculations on bare free-electron metal surfaces[16] showed that the boomerang structure was still visible, although much weakened, in agreement with experimental results on a polycrystalline bare Ag surface.[12] Various reasons can be invoked for these discrepancies. Experimentally, inhomogeneities can be more effective in thin film; the existence of N_2 molecules in different positions on the surface could easily lead to a blurring of the boomerang oscillations. On the theoretical side, one must be reminded that the DCM model is a macroscopic

approach and hence should be valid mainly for thick films and could lead to deficiencies in the case of a very small coverage (e.g., 1 ML).

C. Overtone excitation ratio

The relative magnitude of the fundamental and overtone vibrational levels characterizes the strength of the vibrational excitation process. Overtone excitation is usually considered as the signature of a resonant process and, in the case of a large overtone to fundamental ratio, as the sign of a very-long-lived resonance. However, in the case of adsorbed molecules, the space asymmetry between the vacuum and substrate sides can also play a role.[16]

The overtone excitation ratio is defined, theoretically, as the ratio between energy-integrated summed cross sections and, experimentally, as the ratio between energy-integrated excitation functions. The integration over the energy allows us to get rid of the boomerang interference as well as broadening effects that would not be energy dependent (as energy convolution). Table I presents these ratios as a function of the Ar film thickness:

$$\frac{\int \sigma(0\rightarrow 2)dE}{\int \sigma(0\rightarrow 1)dE}, \quad \frac{\int \sigma(0\rightarrow 3)dE}{\sigma(0\rightarrow 2)dE}.$$

These ratios shows that the overtone excitation is much weaker for N_2 adsorbed on a bare metal surface than for the free molecule. This has been discussed as the combined effect of the decrease of the resonance lifetime and of the space asymmetry introduced by the metal surface[16] (i.e., the effect of the surface barrier due to the image potential interaction). The same reasoning also applies, although to a smaller extent, for N_2 adsorbed on very thin Ar film (1–4 ML). For thicker films (4–32 ML), the overtone excitation ratio is observed, both experimentally and theoretically, to be roughly independent of the thickness.

One could have expected that, owing to the increased resonance lifetime, the overtone excitation would be larger for N_2 adsorbed on an Ar film than for the free molecule. The present results confirm the fact that the resonance lifetime is not the only parameter governing the overtone excitation ratio. For very thin films, one can see in Fig. 2 that the potential barrier at the dielectric-vacuum interface is rather low and somewhat similar to the one found in the bare metal case. So the decrease of the overtone excitation ratio in this case can be tentatively attributed to the effect of the image potential barrier, as in the case of the bare metal surface. For thick films, the potential barrier could also play a role. Another possibility is simply the saturation of the vibrational excitation process, which is already quite strong for the free-molecule situation and cannot increase further. In the limit of a very-long-lived resonance, the vibrational excitation probability at the position of the negative ion vibrational levels is simply given by Franck-Condon factors, which are independent of the resonance lifetime. This feature should make the overtone excitation ratio in N_2 much less sensitive to a decrease of the width than to an increase.

D. Thickness dependence of the excitation cross sections

As can be seen in Fig. 7, the theoretical excitation cross section on the Ar film decreases when the film thickness decreases. This feature can be compared with the experimental data, using the energy-integrated cross sections defined in the previous section. The summed excitation cross sections are found to be proportional to 1, 0.69, and 0.34 for the 16, 8, and 4 ML thicknesses, respectively. The corresponding numbers are 1, 0.87, and 0.57 for the experimental data. The trend is the same, but the calculations overestimate the drop of the excitation cross section. In addition to the points mentioned in the discussion in the previous sections, one can stress that the variation of the magnitude of the excitation cross section with the film thickness is sensitive to the geometry of the adsorption (see Fig. 7).

VIII. CONCLUSION

We have reported on joint theoretical and experimental studies on the resonant vibrational excitation of N_2 molecules by electron impact in the region of the N_2^- ($^2\Pi_g$) resonance. The N_2 molecules were adsorbed on Ar films condensed on a metal substrate. The control of the Ar film thickness allows the investigation of the effect of the environment on the resonant process, from a bare metal to an insulating substrate, by inserting an insulator between the molecule and the metal surface. Experimentally, the resonant process appears to be considerably influenced by its environment.

(i) The resonance structure in the electron energy dependence of the vibrational excitation cross section is strongly perturbed and is shifted toward lower energies: the shift increases as the film thickness decreases. For thick films (i.e., above 4 ML), the shape of the vibrational excitation function is roughly the same, except for an overall energy shift of the resonance structure.

(ii) Below 4 ML the boomerang structure in the experimental vibrational excitation function disappears gradually with decreasing film thickness; on the bare Pt metal, it is completely absent.

(iii) The theoretical results obtained within the CAM formulation, associated with a modeling of the Ar film as a DCM on top of a free-electron metal, reproduce most of the features of the experimental data. It is shown that the main effect of the insulator film is to introduce a potential barrier at the vacuum-dielectric interface, which is partially reflective for resonant electrons. The partial reflectivity of this interface leads to an increase of the N_2^- lifetime, as well as to a modification of the angular distribution of the electrons ejected by resonance decay. This leads to results in agreement with the experimental data for thick Ar films. For thin Ar films, discrepancies between the theoretical and experimental results exist that are tentatively attributed either to the effect of inhomogeneities at the film surface and/or to limitations of the theoretical model.

These studies confirm the ability of resonant scattering by the N_2 molecule to probe the local electronic potential surrounding the molecule. Although the present study was concentrated on the case of Ar film as a model dielectric, one can expect that the present theoretical discussions apply to

all rare gases, with the exception of the differences in the excitation functions and/or overtone excitations at low energies. In this context, solid Ne appears particularly appealing since the conduction-band edge is located around 1.4 eV above the vacuum level. Therefore, a thick Ne film would be practically totally reflecting below this energy and should strongly influence the N_2^- ($^2\Pi_g$) resonance that is lying at about the same energy.

[1] L. Sanche, J. Phys. B **23**, 1597 (1990).
[2] L. Sanche, IEEE Trans. Electr. Insul. **28**, 789 (1993).
[3] R. E. Palmer and P. J. Rous, Rev. Mod. Phys. **64**, 383 (1992).
[4] R. E. Palmer, Prog. Surf. Sci. **41**, 51 (1992).
[5] A. Herzenberg, J. Phys. B **1**, 548 (1968).
[6] D. J. Birtwistle and A. Herzenberg, J. Phys. B **4**, 53 (1971).
[7] J. W. Gadzuk, J. Chem. Phys. **79**, 3982 (1983).
[8] A. Gerber and A. Herzenberg, Phys. Rev. B **31**, 6219 (1985).
[9] P. J. Rous, Surf. Sci. **260**, 361 (1992).
[10] D. Teillet-Billy, V. Djamo, and J. P. Gauyacq, Surf. Sci. **269/270**, 425 (1992).
[11] L. Sanche and M. Michaud, Phys. Rev. Lett. **47**, 4008 (1981).
[12] J. E. Demuth, D. Schmeisser, and Ph. Avouris, Phys. Rev. Lett. **47**, 1166 (1981).
[13] K. Jacobi, C. Astaldi, P. Geng, and M. Bartolo, Surf. Sci. **223**, 569 (1989).
[14] F. Bartolucci, R. Franchy, J. A. M. C. Silva, A. M. C. Moutinho, D. Teillet-Billy, and J. P. Gauyacq, J. Chem. Phys. **108**, 22 512 (1998).
[15] L. Šiller, J. F. Wendelken, K. M. Hock, and R. E. Palmer, Chem. Phys. Lett. **210**, 15 (1993).
[16] V. Djamo, D. Teillet-Billy, and J. P. Gauyacq, Phys. Rev. Lett. **71**, 3267 (1993); Phys. Rev. B **51**, 5418 (1995).
[17] P. J. Rous, Surf. Sci. **279**, L191 (1992).
[18] M. A. Huels, L. Parenteau, and L. Sanche, J. Chem. Phys. **100**, 3940 (1994); P. Rowntree, L. Sanche, L. Parenteau, M. Meinke, F. Weik, and E. Illenberger, *ibid.* **101**, 4248 (1994).
[19] R. Azria, L. Parenteau, and L. Sanche, Phys. Rev. Lett. **59**, 638 (1987); P. Rowntree, L. Parenteau, and L. Sanche, Phys. Rev. Lett. **95**, 4902 (1991); M. A. Huels, P. Rowntree, L. Parenteau, and L. Sanche, Surf. Sci. **390**, 282 (1997).
[20] L. Sanche, A. D. Bass, P. Ayotte, and I. I. Fabrikant, Phys. Rev. Lett. **75**, 3568 (1995).
[21] P. Ayotte, J. Gamache, A. D. Bass, I. I. Fabrikant, and L. Sanche, J. Chem. Phys. **106**, 749 (1997).
[22] M. Bauer, S. Pawlik, and M. Aeschlimann, Phys. Rev. B **55**, 10 040 (1997); **60**, 5016 (1999).
[23] S. Ogawa, H. Nagano, and H. Petek, Phys. Rev. Lett. **82**, 1931 (1999).
[24] A. G. Borisov, A. K. Kazansky, and J. P. Gauyacq, Phys. Rev. Lett. **80**, 1996 (1998); Surf. Sci. **430**, 165 (1999).
[25] D. F. Padowitz, W. R. Merry, C. E. Jordan, and C. B. Harris, Phys. Rev. Lett. **69**, 3583 (1992).
[26] J. D. Mc Neill, R. L. Lingle, R. E. Jordan, D. F. Padowitz, and C. B. Harris, J. Chem. Phys. **105**, 3883 (1996).
[27] A. Hotzel, K. Ishioka, E. Knoesel, M. Wolf, and G. Ertl, Chem. Phys. Lett. **285**, 271 (1998).
[28] A. Hotzel, G. Moos, K. Ishioka, M. Wolf, and G. Ertl, Appl. Phys. B: Lasers Opt. **68**, 615 (1999).
[29] N. J. Sack, M. Akbulut, and T. Madey, Phys. Rev. B **51**, 4585 (1995); Surf. Sci. **334**, L695 (1995).
[30] P. Nordlander and J. P. Modisette, Nucl. Instrum. Methods Phys. Res. B **125**, 305 (1997).
[31] L. Sanche and M. Michaud, Phys. Rev. B **30**, 6078 (1984).
[32] M. Michaud and L. Sanche, J. Vac. Sci. Technol. **17**, 274 (1980).
[33] C. Gaubert, R. Baudoing, Y. Gauthier, M. Michaud, and L. Sanche, Appl. Surf. Sci. **25**, 195 (1986).
[34] M. Michaud, L. Sanche, C. Gaubert, and R. Baudoing, Surf. Sci. **205**, 447 (1988).
[35] M. Michaud and L. Sanche, Phys. Rev. B **30**, 6067 (1984).
[36] L. Sanche and M. Michaud, Phys. Rev. B **27**, 3856 (1983).
[37] L. Dubé and A. Herzenberg, Phys. Rev. A **20**, 194 (1979).
[38] S. F. Wong, results quoted in Ref. 37.
[39] M. Allan (private communication).
[40] D. Teillet-Billy and J. P. Gauyacq, Surf. Sci. **239**, 343 (1990).
[41] B. Bahrim, D. Teillet-Billy, and J. P. Gauyacq, J. Chem. Phys. **104**, 10 014 (1996).
[42] M. W. Cole, Phys. Rev. B **3**, 4418 (1971).
[43] N. Schwentner, E. E. Koch, and J. Jortner, *Electronic Excitations in Condensed Rare Gases* (Springer-Verlag, Berlin, 1985), p. 22; G. Bader, G. Perluzzo, L. G. Caroon, and L. Sanche, Phys. Rev. B **30**, 78 (1984); G. Perluzzo, G. Bader, L. G. Caron, and L. Sanche, Phys. Rev. Lett. **55**, 545 (1985).
[44] N. W. Ashcroft and N. D. Mermin, *Solid State Physics* (Saunders College, Philadelphia, 1976).
[45] P. J. Jennings, P. O. Jones, and M. Weinert, Phys. Rev. B **37**, 6113 (1988).
[46] W. Wurth, G. Rocker, P. Feulner, R. Scheuerer, L. Zu, and D. Menzel, Phys. Rev. B **47**, 6697 (1993).
[47] D. Teillet-Billy and J. P. Gauyacq, J. Phys. B **17**, 4041 (1984).
[48] J. P. Gauyacq, *Dynamics of Negative Ions* (World Scientific, Singapore, 1987).
[49] M. Le Dourneuf, Vo Ky Lan, and J. M. Launay, J. Phys. B **15**, L685 (1982).
[50] V. Djamo, D. Teillet-Billy, and J. P. Gauyacq, Surf. Sci. **346**, 253 (1996).
[51] F. T. Smith, Phys. Rev. **118**, 349 (1960).
[52] J. M. Launay, J. Phys. B **9**, 1823 (1976).
[53] G. Henderson and G. Ewing, Mol. Phys. **27**, 903 (1974).
[54] P. J. Rous, Phys. Rev. Lett. **83**, 5086 (1999).
[55] L. Sanche and M. Michaud, Chem. Phys. Lett. **84**, 497 (1981).
[56] L. Šiller, R. E. Palmer, and J. F. Wendelken, J. Chem. Phys. **99**, 7175 (1993).
[57] S. Lacombe, F. Cemic, P. He, R. Dietrich, P. Geng, M. Rocca, and K. Jacobi, Surf. Sci. **368**, 38 (1996).
[58] D. Teillet-Billy, J. P. Gauyacq, and M. Persson, Phys. Rev. B **62**, R13 306 (2000).